Resiliency-aware Planning of Active Distribution Grids using Multi-parametric Programming

Stavros Karagiannopoulos[§*‡], Stefanos Delikaraoglou[§‡], Gabriela Hug[*], Audun Botterud[§]
[*]EEH - Power Systems Laboratory, ETH Zurich, Physikstrasse 3, 8092 Zurich, Switzerland
[§]Laboratory of Information and Decision Systems, Massachusetts Institute of Technology, Cambridge, MA, USA
Emails: {stavroskarajan, sdelikaraoglou}@gmail.com, audunb@mit.edu, hug@eeh.ee.ethz.ch
[‡]The first two authors contributed equally to this work

***Abstract*—The increasing share of energy resources directly connected at distribution voltage levels and offering local generation capabilities, has enabled distribution grids to operate disconnected from the external main grid. This autonomous mode, whether planned or -most importantly- arising from unintentional events, is commonly referred to as islanded operation. In this paper, we focus on the resilience of active distribution grids in terms of satisfying a certain load share for a specific amount of time in islanded mode. By applying a multi-parametric programming framework to a multi-period optimal power flow problem at the planning stage, we propose a fast resiliency screening method to derive optimal policies for the feasible cases, and to identify all the cases that are infeasible due to violation of resiliency constraints. In a case study on the Cigre low-voltage network, we assess the trade-offs among the available energy storage system (ESS) size, required time duration for safe islanded operation, and the number of infeasible cases. The results of the case study show that the proposed methodology can reduce the computational burden of the resiliency-aware ESS sizing problem, while proving a set of optimal control policies for operation under different uncertainty realizations.**

***Index Terms*—Active distribution grids, Resilience, Multi-parametric optimization, Optimal power flow.**

I. Introduction

Transitioning towards an emission-free and sustainable electricity system, future distribution networks are expected to host increasing shares of distributed energy resources (DERs), mainly solar photovoltaics (PVs) or small-scale wind turbines, and energy storage systems (ESS). The efficient integration of those resources directly at low-voltage networks can promote a larger penetration of renewable energy production, as well as increase the operational flexibility of the distribution grid. On the other hand, the variable and uncertain power production of PV and wind resources introduces various challenges to the distribution grid operation, such as large voltage deviations, line congestions and increased power losses. In view of these emerging issues, the European Distribution System Operators (E.DSO) has underlined the importance of ESS in order to enhance the reliability and resiliency of the future distribution grids [1]. In the same vein, the recent FERC Order No. 2222 establishes a new regulatory framework that enables DERs and ESS to provide new services that enhance grid flexibility and resilience [2].

Over the last years, infrastructure resilience is gaining increased attention in the context of climate change and more extreme weather events. Specifically in the context of power systems, *resiliency* is defined as the ability of the network to withstand the interruption of power supply to critical loads as well as the capability to anticipate, absorb and rapidly recover from these events [3]. Several works in the recent literature study the topic of resiliency in distribution grids considering various extreme events such as windstorms, floods, wildfires, earthquakes and icing [4]–[7]. Here, we pursue an approach similar to [8]–[11], i.e., we study resiliency in distribution grids in view of a generic outage caused by a natural disaster or equipment failure, which causes disconnection from the main transmission system. Considering the islanded operation of the distribution grid, we focus primarily on the planning stage in order to determine the required ESS size that will allow the DSO to reliably supply a certain percentage of the local demand, i.e., defined as critical load, for a certain time horizon defined by the DSO.

Traditionally, DSOs rely on conventional measures, e.g., grid reinforcement, to address security and reliability challenges in distribution networks. Nowadays, the increasing shares of local DERs and ESS provide additional flexibility that is readily available at the local level. These new means of flexibility, given proper planning and operational strategies, can reduce system cost and enhance the reliability of the distribution grid against generation uncertainty, i.e., renewables forecast errors, and equipment contingencies that lead to islanded operation. The problem of optimal sizing and placement of DERs and ESS in distribution systems is studied extensively in the recent literature, e.g., [12]–[15] among others. In terms of resiliency, the work in [16] shows that ESS can improve islanded system reliability under the assumption of perfect PV forecasts. In order to account for the uncertainty of system components, the authors in [17] propose a two-stage probabilistic model for the sizing of ESS in distribution networks, using a heuristic solution approach based on genetic algorithms that does not provide optimality guarantees.

In this work, we follow a different approach for the optimal sizing of ESS under uncertainty. The core components of our proposed method for operation-aware grid planning are the Backward/Forward Sweep (BFS) power flow model [18], and the mathematical concept of multi-parametric programming (MPP) [19] that can reduce the computational burden of our model. MPP is a mathematical technique that enables the exact mapping of the optimal solution to the parameter space, thus providing a systematic way to analyze the impact of variability and uncertainty in mathematical optimization problems. One of the first MPP methods for linear programs is studied in [20] with the goal to find neighboring critical regions,

979-8-3315-1278-1/25/$31.00

i.e., subsets of the parameter space with different optimal basis, by visiting iteratively the graph of bases associated with the Simplex tableau of the original problem. Here, we follow the geometric approach presented in [21] in which critical regions are defined in terms of active constraints. In the context of power systems, [22] and [23] have used MPP for forecasting electricity market prices, whereas [24] applies MPP in security-constrained economic dispatch. The MPP framework is also applied in [25] for statistical learning of the DC optimal power flow (OPF) problem. Finally, the applications of MPP in distribution grids is rather limited, with the exception of reference [26], where MPP is used for accelerating the probabilistic hosting capacity analysis for DER in the low voltage network.

The contribution of this paper is threefold:

- The development of a novel decision-support tool to assist DSOs in the task of resiliency-aware planning and ESS investment decisions in view of operational uncertainties.
- The application of the MPP theory on a multi-period optimal power flow model that enables the derivation of optimal control policies and fast resiliency assessment in active distribution grids.
- The trade-off assessment between additional ESS capacity and distribution system resiliency in terms of magnitude and duration of critical load satisfaction.

The rest of the paper is organized as follows. Section II outlines the main theory of multi-parametric programming, and describes the proposed methodology for the derivation of optimal policies and the fast resiliency assessment process in active distribution grids. Section III introduces the case study and discusses the results in terms of computational gains from the application of the MPP theory as well as the trade-offs between enhanced resiliency and ESS investment decisions. Finally, Section IV concludes the paper.

II. Methodology

This section presents the core components of our methodology. First, we present the main principles of the MPP theory (Sec. II-A). Then, we describe the proposed decision-support tool for the optimal sizing of ESS by the DSO, taking into account system uncertainties as well as planning and operational decision parameters. The detailed multi-period BFS-OPF model is presented in the Appendix (Sec. V-B).

A. Multi-parametric programming

Here, we provide the main concepts of multi-parametric programming, following the theory from [21]. Let us consider a general formulation of a right-hand side multi-parametric program as follows:

$$\mathcal{Q}(\mathbf{z}) = \underset{\mathbf{x}}{\text{Minimize}} \quad \mathbf{c}^\intercal \mathbf{x} \tag{1a}$$

subject to

$$\mathbf{G}\mathbf{x} \leq \mathbf{W} + \mathbf{S}\mathbf{z} \;:\; \boldsymbol{\mu}. \tag{1b}$$

The objective function is a linear function of variables $\mathbf{x} \in \mathbb{R}^\kappa$ with the corresponding cost vector being $\mathbf{c} \in \mathbb{R}^\kappa$. All constraints are linear and $\mathbf{z} \in \mathbb{R}^d$ denotes the parameters vector. Accordingly, the constraint matrices have dimensions $\mathbf{G} \in \mathbb{R}^{m\times\kappa}$, $\mathbf{W} \in \mathbb{R}^m$ and $\mathbf{S} \in \mathbb{R}^{m\times d}$. For any given $\mathbf{z} \in \mathcal{Z}$, denote as $\mathcal{Q}^*(\mathbf{z})$, $\mathbf{x}^*(\mathbf{z})$ and $\mathcal{M}^*(\mathbf{z})$ the optimal objective value and the sets of optimal primal and dual solutions of problem (1), respectively.

For a closed and bounded polyhedral set $\mathcal{B} \subseteq \mathbb{R}^d$, denote by $\mathcal{Z} \subseteq \mathcal{B}$ the region of parameters $\mathbf{z} \in \mathcal{Z}$ for which (1b) is feasible, i.e., $\mathcal{Z} = \{\mathbf{z} \in \mathcal{B} : \exists\ \mathbf{x} \mid \mathbf{G}\mathbf{x} \leq \mathbf{W} + \mathbf{S}\mathbf{z}\}$. Let $\mathcal{J} = \{1, \ldots, m\}$ denote the set of constraint indices in (1b) and for any subset $\mathcal{I} \subseteq \mathcal{J}$, the submatrices of $\mathbf{G}$, $\mathbf{W}$ and $\mathbf{S}$ whose rows are indexed by $\mathcal{I}$ are denoted as $\mathbf{G}_\mathcal{I}$, $\mathbf{W}_\mathcal{I}$ and $\mathbf{S}_\mathcal{I}$, respectively. An optimal partition $(\mathcal{J}^{\text{A}}(\mathbf{z}), \mathcal{J}^{\text{NA}}(\mathbf{z}))$ of set $\mathcal{J}$ associated with the parameter vector $\mathbf{z} \in \mathcal{Z}$ is defined as:

$$\mathcal{J}^{\text{A}}(\mathbf{z}) = \{j \in \mathcal{J} \mid \mathbf{G}_j\mathbf{x}(\mathbf{z}) = \mathbf{W}_j + \mathbf{S}_j\mathbf{z}\}, \tag{2a}$$

$$\mathcal{J}^{\text{NA}}(\mathbf{z}) = \{j \in \mathcal{J} \mid \mathbf{G}_j\mathbf{x}(\mathbf{z}) < \mathbf{W}_j + \mathbf{S}_j\mathbf{z}\}, \tag{2b}$$

where the index sets $\mathcal{J}^{\text{A}}$ and $\mathcal{J}^{\text{NA}}$ correspond to active and inactive constraints at the optimum of problem (1). This definition is valid under the assumption that problem (1) is neither primal nor dual degenerate, i.e., there exists a unique optimal primal and dual solution for all $\mathbf{z} \in \mathcal{Z}$.

For a given $\mathbf{z}_0 \in \mathcal{Z}$, let $(\mathcal{J}_0^{\text{A}}, \mathcal{J}_0^{\text{NA}}) = (\mathcal{J}^{\text{A}}(\mathbf{z}_0), \mathcal{J}^{\text{NA}}(\mathbf{z}_0))$, then the corresponding *critical region* $\mathcal{CR}_0$ is defined as:

$$\mathcal{CR}_0 = \{\mathbf{z} \in \mathcal{Z} \mid \mathcal{J}^{\text{A}}(\mathbf{z}) = \mathcal{J}_0\}, \tag{3}$$

which is the set of all parameters $\mathbf{z} \in \mathcal{Z}$ for which the set $\mathcal{J}_0^{\text{A}}$ of constraints is the same at the optimal solution. For the linear programming problem (1) the critical region is given by:

$$\begin{aligned}\mathcal{CR}_0 = \{\mathbf{z} \in \mathcal{Z} \mid &(\mathbf{G_{NA}}\mathbf{G_A^{-1}}\mathbf{S_A} - \mathbf{S_{NA}})\mathbf{z} < \\ &\mathbf{W_{NA}} - \mathbf{G_{NA}}\mathbf{G_A^{-1}}\mathbf{W}_A\}.\end{aligned} \tag{4}$$

Full dimensional critical regions are described by k active constraints. If the problem is not primal or dual degenerate, the sets of active constraints $\mathcal{J}^{\text{A}}$ and $\tilde{\mathcal{J}}^{\text{A}}$ of two neighbouring full-dimensional critical regions $\mathcal{CR}_0$ and $\tilde{\mathcal{CR}}_0$ differ only by one constraint. In other words, as one constraint becomes inactive, another new constraint becomes active. However, if primal degeneracy occurs, critical regions may be described by more than k constraints, and vice versa for dual degeneracy.

In the open polyhedron (4), the optimal primal solution $\mathbf{x}^*(\mathbf{z})$ and the objective function $\mathcal{Q}^*(\mathbf{z})$ are given as affine functions of the parameter $\mathbf{z}$ as

$$\mathbf{x}^*(\mathbf{z}) = \mathbf{G_A^{-1}}\mathbf{S_A}\mathbf{z} + \mathbf{G_A^{-1}}\mathbf{W_A}, \tag{5}$$

$$\mathcal{Q}^*(\mathbf{z}) = \mathbf{c}^\intercal\mathbf{G_A^{-1}}(\mathbf{W_A} + \mathbf{S_A}\mathbf{z}), \tag{6}$$

whereas the dual variables are constant, i.e., $\boldsymbol{\mu}^*(\mathbf{z}) = \boldsymbol{\mu}(\mathbf{z}_0)$.

Using the multi-parametric programming framework described above allows us to pre-compute and store the result of the optimization process in the form of an analytical function that can be readily evaluated for different values of the input parameters $\mathbf{z}$. Hence, we can obtain explicitly the mappings from the parameter space $\mathcal{Z}$ to the set of primal and dual optimal solution sets, without repeatedly solving the optimization problem (1) for all $\mathbf{z} \in \mathcal{Z}$.

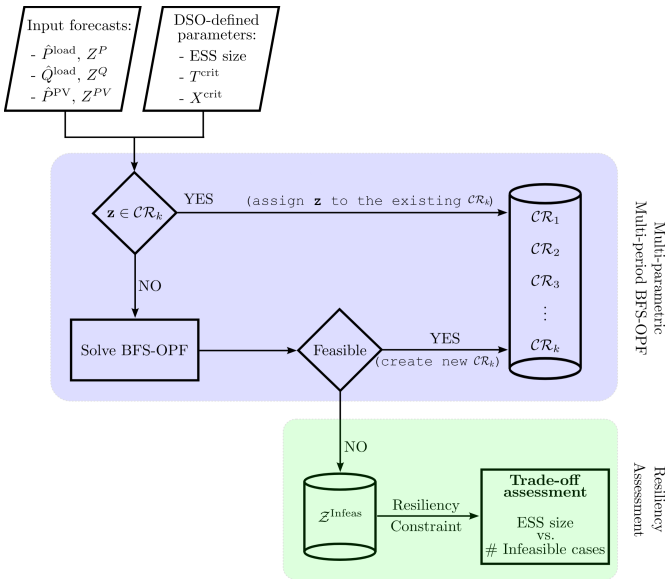

Fig. 1. Proposed methodology considering the resiliency-aware multi-parametric multi-period BFS-OPF.

B. Optimal Policies and Fast Resiliency Assessment for Planning in Active Distribution Grids

The proposed method for optimal sizing the ESS to enhance the resiliency of the distribution system during islanded operation, is based on the integration of the multi-period BFS-OPF into the MPP framework. In this work, the set of parameters $\mathcal{Z}$ denotes the forecast error from the expected value of active and reactive demand, denoted as $\hat{P}^{\text{load}}_{nt}$ and $\hat{Q}^{\text{load}}_{nt}$, respectively, and the expected PV production $\overline{P}_{nt}$ that are considered as random variables subject to uncertainties. Consequently, the parameter set $\mathcal{Z}$ comprises vectors $Z^{\text{P}}_{ntz}, Z^{\text{Q}}_{ntz}$ and Z^{PV}_{ntz} that define the deviation from the expected value for active/reactive demand and PV production, respectively.

In order to include the forecast error parameter errors within set $\mathcal{Z}$ into the multi-period BFS-OPF model (1), the problem is reformulated as follows:

$$\underset{\Xi^{\text{Z}}}{\text{Minimize}} \sum_{t} \Big[\sum_{n} C^{\text{P}}_{n} p_{ntz} + \sum_{n} C^{\text{Q}}_{n} (q^{+}_{ntz} - q^{-}_{ntz}) \Big] \Delta T \quad (7a)$$

subject to

$$\text{constraints (8b), (8f)} - \text{(8n)} \quad (7b)$$

$$p^{\text{inj}}_{ntz} = p_{ntz} + p^{\text{st}}_{ntz} - \hat{P}^{\text{load}}_{nt} + Z^{\text{P}}_{ntz}, \ \forall n, t \quad (7c)$$

$$q^{\text{inj}}_{ntz} = q_{ntz} - \hat{Q}^{\text{load}}_{nt} + Z^{\text{Q}}_{ntz}, \ \forall n, t \quad (7d)$$

$$\underline{P}_{n} \leq p_{ntz} \leq \hat{P}_{nt} + Z^{\text{PV}}_{ntz}, \ \forall n, t \quad (7e)$$

$$\sum_{n \in \mathcal{N}/n_1} e_{n\tau z} \geq \sum_{t=\tau}^{\tau+T^{\text{crit}}} \sum_{n \in \mathcal{N}/n_1} X^{\text{crit}} \cdot \Big[(\hat{P}^{\text{load}}_{nt} + Z^{\text{P}}_{ntz}) - (\overline{P}_{nt} + Z^{\text{PV}}_{ntz}) \Big] \Delta T, \forall t \quad (7f)$$

where $\Xi^{\text{Z}} = \{p_{ntz}, p^{\text{inj}}_{ntz}, q_{ntz}, q^{\text{inj}}_{ntz}, q^{+}_{ntz}, q^{-}_{ntz}, v_{ntz}, p^{\text{st}}_{ntz}, e_{ntz}, \forall n, t, z; \ \ i_{\ell tz}, \forall \ell, t, z\}$ is the set of optimization variables augmented by index z that denotes the elements of set $\mathcal{Z}$.

Figure 1 illustrates the different steps of the ESS sizing process, which takes as inputs the local demand and production forecasts (expected values and forecast errors in set $\mathcal{Z}$), the DSO-defined parameters that pertain to the ESS size $\overline{P}^{\text{st}}_{nt}$ and $\overline{P}_{nt}$ as well as the percentage and the duration of critical load, X^{crit} and T^{crit}, respectively. For each $\mathbf{z} := \{Z^{\text{P}}_{ntz}, Z^{\text{Q}}_{ntz}, Z^{\text{PV}}_{ntz}\} \in \mathcal{Z}$, using the critical region definition in (4), we check if this $\mathbf{z}$ falls within one of the critical regions $\mathcal{CR}_k$, where $k \in \mathcal{K}$ is the index of critical regions that have already been discovered in the course of the algorithm. If the current $\mathbf{z}$ belongs to an already discovered critical region, it is assigned to $\mathcal{CR}_k$ and the algorithm proceeds with the next z. If no $\mathcal{CR}_k$ in the library of critical regions include z, then we invoke the BFS-OPF model (7a) to obtain a new solution and identify the new critical region $\mathcal{CR}_{k'}$ that is then added to the library $\mathcal{CR}_k, \ k \in \mathcal{K} \cup k'$. If at this step, the BFS-OPF model proves to be infeasible due to the resiliency constraint, the current $\mathbf{z}$ is assigned to the library of infeasible parameters $\mathcal{Z}^{\text{Infeas}}$. The algorithm terminates once all $\mathbf{z} \in \mathcal{Z}$ are examined.

In the case of primal degeneracy, the assignment of a realization vector $\mathbf{z}$ to a specific critical region is not important because multiple optimal solutions can correspond to the same $\mathbf{z}$. Consequently, we allow the solver to arbitrarily select the set of active constraints for mapping this $\mathbf{z}$ into the dictionary of discovered critical regions. Alternatively, degenerate instances can be uniquely assigned to specific critical regions by using a tie-braking rule, as discussed in [25].

The method described above can serve as a decision-support tool for the DSO in order to assess the trade-off between the ESS size and the number of infeasible cases for different values of the operational parameters X^{crit} and T^{crit}. From a computational perspective, the MPP framework allows to assess the system behavior for a large range of the uncertainty, i.e., a high cardinality of parameter set $\mathcal{Z}$, without solving the multi-period BFS-OPF model for every $\mathbf{z} \in \mathcal{Z}$. In addition, this approach readily provides to the DSO the optimal control policies and the corresponding costs, according to (5) and (6), respectively, within each critical region. This information can be leveraged by the DSO at the operational stage.

III. Case Study

A. Network parameters and input data

In order to demonstrate the proposed method, we use a typical European radial LV grid [27], sketched in Fig. 2. is modeled using a single phase representation, but the framework can be extended to three-phase unbalanced networks as explained in [28]. We consider PV units with installed capacity of 30 kW at nodes 12, 17, 18 and 19, and an ESS unit located at node 2. In the initial system configuration, the maximum ESS capacity is 400 kWh, whereas its maximum charge/discharge power is set to 400 kW. The state of charge at the beginning and the end of the optimization horizon is set to 1, i.e., 400 kWh to highlight the paper's focus on resiliency. In terms of network constraints, we set the minimum and the maximum acceptable voltage to 0.96 p.u. and 1.04 p.u., respectively, at every node of the system. The maximum allowable current magnitude for all cables of the distribution network is set to 1 p.u. (with respect to the cable base).

With regard to the net load uncertainty modeling, we assume that the forecast error distribution for the active and reactive power demand at the different nodes, i.e., parameters $Z^{\text{P}}_{ntz}, Z^{\text{Q}}_{ntz}$ that appear in constraints (7c), (7d), (7e) and (7f), follow a Gaussian distribution $\mathcal{N}(\mu, \sigma^2)$. We set the mean $\mu = 0$ and we examine different values of the variance σ^2

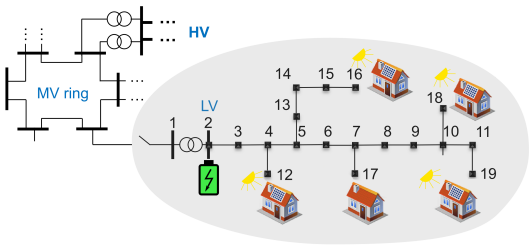

Fig. 2. Cigre residential European LV grid able to operate in both grid-connected and islanded mode.

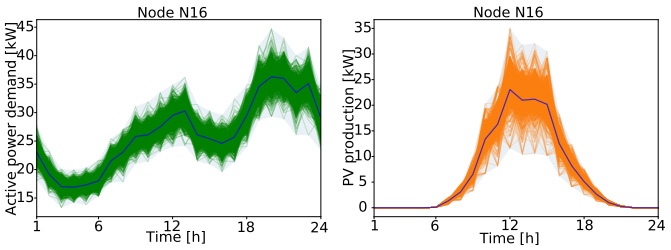

Fig. 3. Active power demand and PV production at node 16: Uncertainty envelope, base case profile and the subset of parametric scenarios that belong to the largest base.

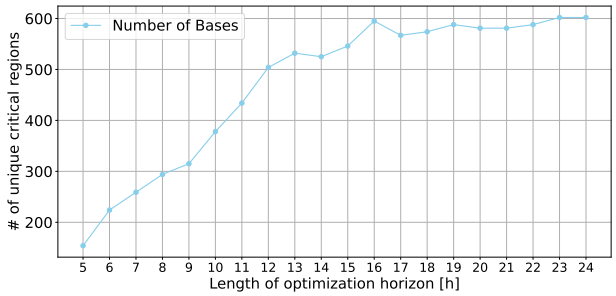

Fig. 4. Number of bases as a function of the considered optimization horizon.

for each time-step of the forecast trajectory, in order to assess the impact of different levels of uncertainty in our proposed methodology. In turn, PV production forecast errors are modelled using historical forecast error distributions based on real data in Switzerland [29]. These forecast error distributions correspond to the parameters Z^{PV}_{ntz} in (7e) and (7f). Given the limited geographical dispersion of PV installations in the distribution network, we consider that PV power production at the different nodes exhibits perfect spatial correlation, i.e., all PV units follow the same forecast error distribution.

B. MPP-based control policies accounting for operational uncertainties

In this part, we focus on the multi-period BFS-OPF implementation using the multi-parametric programming framework (see the upper part of Fig. 1) and we elaborate on the benefits of the proposed MPP-based methodology for the derivation of optimal control policies, as well as for the reduction of the computational burden in view of operational uncertainties. The results presented below are derived setting the parameter $X^{\text{crit}} = 0.4$ and using 1000 parametric cases that correspond to different plausible realizations of active and reactive power demand, and PV production.

1) Limited uncertainty range - Current operating conditions: In order to assess the proposed methodology under current operating conditions with low shares of installed DERs that induce limited uncertainty and variability in system operation, we set the variance of the forecast error distribution equal to $\sigma^2 = 0.15$ p.u. for both active and reactive nodal demands. This setting resembles the prevailing operational state of distribution networks, where load uncertainty is limited around the expected value and few active components, e.g., electric vehicles, are present in the low voltage networks.

Fig. 3 show the base case profiles for the active power demand, and the PV power profile for Node 16, respectively. In each plot, the gray shaded area represents the uncertainty envelope derived from 1000 scenarios, bounded by the upper and lower limits of uncertainty at each time step. The green and the orange curves in Fig. 3 illustrate the parametric scenarios ($Z^{\text{P}}tz$ and Z^{PV}_{tz}, respectively) that belong to the largest critical region $\mathcal{CR}$, defined as the critical region containing the highest number of parametric scenarios. The bold lines within the uncertainty envelopes denote the base case profiles. According to the mathematical definitions of multi-parametric programming outlined in Section II-A, the optimal system response to all these scenarios is provided by the same policy.

In view of this uncertainty range, the considered distribution system operates within its limits and none of the uncertainty realizations lead to infeasible cases. Moreover, the number of distinct critical regions for the full 24-hour optimization horizon is limited to three, allowing the DSO to operate the distribution network in an optimal manner by activating one of the three control policies according to the specific uncertainty realization and the bounds of each critical region. This feature brings also a considerable computational advantage to the DSO also in the planning phase, given that only three instances of the multi-period BFS-OPF have to actually be solved, instead of the full set of 1000 $\mathbf{z}$-parametrized models.

2) Large uncertainty range - Future operating conditions: The behavior of active distribution grids is expected to change drastically due to the increasing penetration of local PV units, household-based ESS, uncoordinated charging and discharging of electric vehicles and participation of individual consumers in demand response programs. As a result, a major challenge that emerges for modern DSOs is to forecast accurately the household load patterns and guarantee security of supply to the end customers in the presence of significantly larger uncertainty ranges. Aiming to assess the resiliency of the distribution network under more stressed operating conditions in terms of uncertainty and variability, we set hereinafter the variance of the forecast error distributions of the active and reactive power demand equal to $\sigma^2 = 0.6$ p.u. and we double the installed PV capacity.

In order to quantify the computational gains from the application of the MPP multi-period BFS-OPF framework for varying lengths of the optimization horizon defined by the DSO, we plot in Fig. 4 the total number of unique critical regions, as the optimization horizon increases from 5 to 24 hours. These values provide an estimate about the potential reduction of computational burden for the problem at hand, based on the unbiased metric of the total number of optimizer calls. It should be noted, however, that the actual computational time may vary depending upon the specific implementation (e.g. sequential or parallel solution of each BFS-OPF model instance) and available computational capabilities.

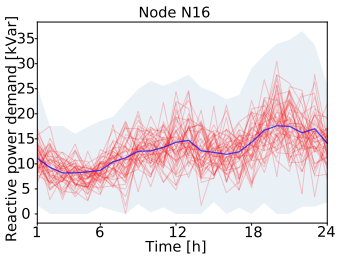

Fig. 5. Reactive power demand at node 16 for large uncertainty range: Uncertainty envelope, base case profile and the subset of infeasible parametric scenarios.

We observe that the number of unique critical regions increases as the optimization horizon increases from 5 to 24 hours and the problem becomes more complex. For the final 24-hour optimization horizon, 600 critical regions are derived, which corresponds to 60% of the scenario set. Overall, the MPP framework reduces the needed computational effort by 50% for optimization horizon of 12 hours, whereas it can achieve around 40% lower computational times for optimization horizons of 16 to 24 hours. This observation allows the DSO to consider a trade-off between the computational time of the MPP-based multi-period BFS-OPF model and the optimization horizon, e.g., employing more frequent re-optimization with shorter look-ahead time, both on the operational and the planning stages, depending on specific applications and system needs.

C. Resiliency assessment

In order to provide a better intuition about the resiliency assessment component of the proposed decision-support tool, Fig. 5 shows the parametric scenarios for the large uncertainty range that lead to infeasible instances of the multi-period BFS-OPF model. It is worth noting that these parametric scenarios cause constraint violations that the current system setup is unable to handle, despite the fact that the respective values may be far from the bounds of the uncertainty envelope. This observation highlights the increased complexity brought by the resiliency constraint, which couples consecutive time periods of the optimization problem.

Continuing the above analysis based on the infeasible parametric uncertainty trajectories, we investigate the alternative operational and system reinforcement that the DSO may consider to reach feasibility and enhance the resiliency of its distribution network according to the lower part of Fig. 1.

Figure 6 (left) provides a trade-off assessment between planning decisions in terms of installing additional ESS capacity to increase the total storage capabilities, and operational settings provided by the DSO in terms of commitment to lower critical load satisfaction (X^{crit}). With T^{crit} fixed to 5 hours, we observe that for an ESS capacity larger than 0.36 MWh and a critical load to be served smaller than or equal to 45%, the distribution system is able to withstand every uncertainty realization in islanded mode. This is illustrated with the blue points that do not result in infeasible cases. On the other hand, lowering the ESS size, or increasing the critical load requirements leads to higher numbers of infeasible cases and diminishes the resiliency capabilities of the system. This is illustrated with the red points that correspond to non-zero infeasible cases.

Similar conclusions can be drawn from Fig. 6 (right) that investigates the number of infeasible parametric scenarios as

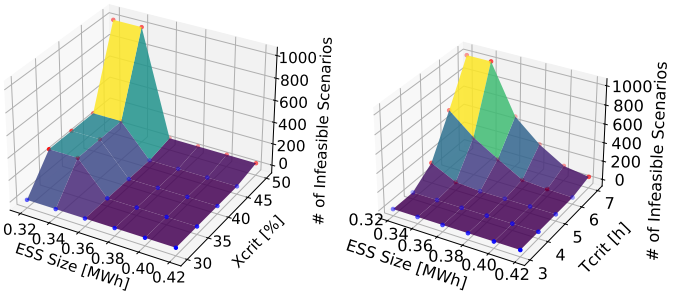

Fig. 6. Number of infeasible cases as a function of the percentage (right) and the duration (left) of critical load (X^{crit}) and ESS size, for T^{crit} = 5 hours (right), and $X^{\text{crit}} = 0.4$ (left).

a function of the committed duration (T^{crit}) of critical load satisfaction and the ESS size, for a fixed $X^{\text{crit}} = 0.4$. The system is able to withstand any uncertainty realization for T^{crit} lower than 5 hours, even with small ESS capacities. On the other hand, higher values of T^{crit}, require higher ESS installed capacity, since the local available generation is not sufficient to cover the demand during certain intervals and provide enough energy to the ESS to cover the critical load ($X^{\text{crit}} = 0.4$). This analysis readily provides important insights to the disconnected grids regarding the maximum acceptable timeframe to restore the connection to the main network.

Although the general conclusions from these figures confirm the common engineering intuition, the proposed methodology offers DSOs a decision-support tool that can assist them in several ways. First, they can quantify the probability of being able to guarantee resiliency, i.e., the number of feasible cases over the full parametric scenario set. Second, based on the specific characteristics of each network in terms of constraint violations, it offers a planning tool to decide on the investment in additional ESS, or reducing the time horizon and/or critical load to reach specific resiliency goals.

IV. Conclusion

Given the growing installations of distributed energy resources, DSOs require innovative tools to ensure the resilient operation of their networks during islanded conditions. This paper formulates a resiliency-aware planning decision-support tool that combines multi-parametric programming with multi-period BFS-OPF to account for the inter-temporal constraints that govern ESS operation and model different resiliency components. The considered case studies show that the proposed tool is capable of reducing the computational burden that arises from the requirement of accurately modelling the operational uncertainties involved in the ESS sizing problem, especially for limited uncertainty ranges, or shorter optimization horizons. In addition, the results illustrate the relationship between the ESS size and different resiliency requirements, i.e., defined to be the guaranteed duration of islanded operation and percentage of critical load satisfaction. This enables the DSO to assess the trade-offs between higher ESS investments and the resulting resiliency gains. Finally, the application of multi-parametric programming readily provides the optimal control policies for different uncertainty realizations, which can be used by the DSO also in the dispatch phase eliminating the need for repeated solutions of the full optimization problem.

Future work may focus on enhanced modelling of the AC power flow equations using alternative approximation/convexification techniques.

REFERENCES

[1] European Distribution System Operators. https://www.edsoforsmartgrids.eu/. Accessed: 2020-09-29.

[2] FERC Order No. 2222: A New Day for Distributed Energy Resources. https://www.ferc.gov/media/ferc-order-no-2222-fact-sheet. Accessed: 2020-09-29.

[3] A. Stankovic and K. Tomsovic, "The definition and quantification of resilience," *IEEE PES Industry Technical Support Task Force*, pp. 1–4, 2018.

[4] S. Espinoza, M. Panteli, P. Mancarella, and H. Rudnick, "Multi-phase assessment and adaptation of power systems resilience to natural hazards," *Electr. Power Syst. Res.*, vol. 136, pp. 352–361, 2016.

[5] M. Panteli, C. Pickering, S. Wilkinson, R. Dawson, and P. Mancarella, "Power system resilience to extreme weather: fragility modeling, probabilistic impact assessment, and adaptation measures," *IEEE Trans. Power Syst.*, vol. 32, no. 5, pp. 3747–3757, 2016.

[6] X. Liu, M. Shahidehpour, Z. Li, X. Liu, Y. Cao, and Z. Bie, "Microgrids for enhancing the power grid resilience in extreme conditions," *IEEE Trans. Smart Grid*, vol. 8, no. 2, pp. 589–597, 2016.

[7] J. Najafi, A. Peiravi, A. Anvari-Moghaddam, and J. M. Guerrero, "Resilience improvement planning of power-water distribution systems with multiple microgrids against hurricanes using clean strategies," *J. Clean. Prod*, vol. 223, pp. 109–126, 2019.

[8] K. Balasubramaniam, P. Saraf, R. Hadidi, and E. B. Makram, "Energy management system for enhanced resiliency of microgrids during islanded operation," *Electr. Power Syst. Res.*, vol. 137, pp. 133–141, 2016.

[9] G. Huang, J. Wang, C. Chen, J. Qi, and C. Guo, "Integration of preventive and emergency responses for power grid resilience enhancement," *IEEE Trans. Power Syst.*, vol. 32, no. 6, pp. 4451–4463, 2017.

[10] A. Hussain, V.-H. Bui, and H.-M. Kim, "Optimal operation of hybrid microgrids for enhancing resiliency considering feasible islanding and survivability," *IET Renew. Power Gener.*, vol. 11, no. 6, pp. 846–857, 2017.

[11] S. Karagiannopoulos, J. Gallmann, M. G. Vayá, P. Aristidou, and G. Hug, "Active distribution grids offering ancillary services in islanded and grid-connected mode," *IEEE Trans. Smart Grid*, vol. 11, no. 1, pp. 623–633, 2019.

[12] E. Grover-Silva, R. Girard, and G. Kariniotakis, "Optimal sizing and placement of distribution grid connected battery systems through an socp optimal power flow algorithm," *Appl. Energy*, vol. 219, pp. 385–393, 2018.

[13] M. Nick, M. Hohmann, R. Cherkaoui, and M. Paolone, "Optimal location and sizing of distributed storage systems in active distribution networks," in *2013 IEEE Grenoble Conference*. IEEE, 2013, pp. 1–6.

[14] R. Johnson, M. Mayfield, and S. Beck, "Optimal placement, sizing, and dispatch of multiple bes systems on uk low voltage residential networks," *J. Energy Storage*, vol. 17, pp. 272–286, 2018.

[15] P. Fortenbacher, M. Zellner, and G. Andersson, "Optimal sizing and placement of distributed storage in low voltage networks," in *2016 Power Systems Computation Conference (PSCC)*. IEEE, 2016, pp. 1–7.

[16] J. Zhou, S. Tsianikas, D. P. Birnie III, and D. W. Coit, "Economic and resilience benefit analysis of incorporating battery storage to photovoltaic array generation," *Renew. Energy*, vol. 135, pp. 652–662, 2019.

[17] A. S. Awad, T. H. El-Fouly, and M. M. Salama, "Optimal ess allocation and load shedding for improving distribution system reliability," *IEEE Trans. Smart Grid*, vol. 5, no. 5, pp. 2339–2349, 2014.

[18] J.-H. Teng, "A direct approach for distribution system load flow solutions," *IEEE Trans. Power Del.*, vol. 18, no. 3, pp. 882–887, 2003.

[19] F. Borrelli, A. Bemporad, and M. Morari, "Geometric algorithm for multiparametric linear programming," *J. Optimiz. Theory App.*, vol. 118, no. 3, pp. 515–540, 2003.

[20] T. Gal and J. Nedoma, "Multiparametric linear programming," *Management Sci.*, vol. 18, no. 7, pp. 406–422, 1972.

[21] F. Borrelli, A. Bemporad, and M. Morari, *Predictive control for linear and hybrid systems*. Cambridge University Press, 2017.

[22] Q. Zhou, L. Tesfatsion, and C.-C. Liu, "Short-term congestion forecasting in wholesale power markets," *IEEE Trans. Power Syst.*, vol. 26, no. 4, pp. 2185–2196, 2011.

[23] Y. Ji, R. J. Thomas, and L. Tong, "Probabilistic forecasting of real-time lmp and network congestion," *IEEE Trans. Power Syst.*, vol. 32, no. 2, pp. 831–841, 2016.

[24] A. N. Madavan, S. Bose, Y. Guo, and L. Tong, "Risk-sensitive security-constrained economic dispatch via critical region exploration," in *2019 IEEE Power & Energy Society General Meeting (PESGM)*. IEEE, 2019, pp. 1–5.

[25] Y. Ng, S. Misra, L. A. Roald, and S. Backhaus, "Statistical learning for DC optimal power flow," in *2018 Power Systems Computation Conference (PSCC)*. IEEE, 2018, pp. 1–7.

[26] S. Taheri, M. Jalali, V. Kekatos, and L. Tong, "Fast probabilistic hosting capacity analysis for active distribution systems," *IEEE Trans. Smart Grid*, 2020.

[27] K. Strunz, E. Abbasi, C. Abbey, C. Andrieu, F. Gao, T. Gaunt, A. Gole, N. Hatziargyriou, and R. Iravani, "Benchmark Systems for Network Integration of Renewable and Distributed Energy Resources," *CIGRE, Task Force C6.04*, no. 273, pp. 4–6, 4 2014.

[28] S. Karagiannopoulos, P. Aristidou, and G. Hug, "Data-driven local control design for active distribution grids using off-line optimal power flow and machine learning techniques," *IEEE Trans. Smart Grid*, vol. 10, no. 6, pp. 6461–6471, 2019.

[29] Federal office of meteorology and climatology. http://www.meteosuisse.admin.ch/. Accessed: 2020-05-30.

V. Appendix

A. Nomenclature

The main notation used in this paper is stated below. Additional symbols are defined in the paper where needed. All symbols are augmented by index t when referring to different time periods.

1) Sets and Indices:

$n \in \mathcal{N}$	Set of nodes.
$t \in \mathcal{T}$	Set of time periods.
$\ell \in \mathcal{L}$	Set of branches, i.e., lines/cables.

2) Parameters:

BIBC	Network topology matrix mapping the bus-injection currents to the branch currents.
BCBV	Matrix of complex impedance of the branches.
$C_n^{\mathrm{P}}, C_n^{\mathrm{Q}}$	Cost of active/reactive power at node n [\$/kWh]
$\overline{E}_n, \underline{E}_n$	Max/min state of charge of storage located at node n [kWh].
$\overline{P}_n, \underline{P}_n$	Max/min active power generation at node n [kW].
$\underline{P}_n^{\mathrm{st}}, \overline{P}_n^{\mathrm{st}}$	Maximum (dis)charging power of ESS [kW].
$\overline{Q}_n, \underline{Q}_n$	Max/min reactive power generation at node n [kVar].
P_n^{load}	Active power demand at node n [kW].
Q_n^{load}	Reactive power demand at node n [kVar].
V_n^*	Known voltage magnitudes of the previous backward forward sweep power flow iteration [V].
T^{crit}	Duration of critical load satisfaction [h].
X^{crit}	Critical load defined as percentage of the total load to be served in islanded mode [%].

3) Decision variables:

e_n	State of charge of ESS located at node n [kWh].
p_n	Active power production at node n [kW].
p_n^{st}	Active power injection/absorption from ESS located at node n [kW].
q_n	Reactive power production at node n [kVar].
q_n^+ / q_n^-	Auxiliary variables for minimization of reactive power [kVar].
v_n	Voltage at node n [V].
i_ℓ	Current flow in branch ℓ [Amp].
p_n^{inj}	Net active power injection at node n [kW].
q_n^{inj}	Net reactive power injection at node n [kVar].

B. Multi-period BFS-OPF

The multi-period OPF problem using the BFS power flow formulation from [15] is modeled as follows:

$$\underset{\Xi}{\text{Minimize}} \quad \sum_t \Big[\sum_n C_n^{\mathrm{P}} p_{nt} + \sum_n C_n^{\mathrm{Q}} (q_{nt}^+ + q_{nt}^-) \Big] \Delta T \quad (8a)$$

subject to

$$q_{nt} = q_{nt}^+ - q_{nt}^-,\ q_{nt}^+, q_{nt}^- \geq 0\ \forall n, t \quad (8b)$$

$$p_{nt}^{\mathrm{inj}} = p_{nt} + p_{nt}^{\mathrm{st}} - P_{nt}^{\mathrm{load}},\ \forall n, t \quad (8c)$$

$$q_{nt}^{\mathrm{inj}} = q_{nt} - Q_{nt}^{\mathrm{load}},\ \forall n, t \quad (8d)$$

$$\underline{P}_n \leq p_{nt} \leq \overline{P}_{nt},\ \forall n, t \quad (8e)$$

$$\underline{Q}_n \leq q_{nt} \leq \overline{Q}_n,\ \forall n, t \quad (8f)$$

$$i_{\ell t} = -\sum_n \mathrm{BIBC}(\ell, n) \cdot p_{nt}^{\mathrm{inj}} / |V_n|,\ \forall \ell, t \quad (8g)$$

$$-\overline{I}_\ell \leq i_{\ell t} \leq \overline{I}_\ell,\ \forall \ell, t \quad (8h)$$

$$v_{nt} = \sum_\ell \sum_n Re\{\mathrm{BCBV}(\ell, n)\mathrm{BIBC}(\ell, n) \cdot p_{nt}^{\mathrm{inj}} / |V_n|\} + V_1 \qquad \forall n, t \quad (8i)$$

$$\underline{V}_n \leq v_{nt} \leq \overline{V}_n,\ \forall n, t \quad (8j)$$

$$e_{nt} = e_{n,t-1} + p_{nt}^{\mathrm{st}} \Delta T,\ \forall n, t \quad (8k)$$

$$e_{nt} = e_n^0,\ \forall n, t = 0 \text{ and } t = T \quad (8l)$$

$$\underline{E}_n \leq e_{nt} \leq \overline{E}_n,\ \forall n, t \quad (8m)$$

$$\underline{P}_{nt}^{\mathrm{st}} \leq p_{nt}^{\mathrm{st}} \leq \overline{P}_{nt}^{\mathrm{st}},\ \forall n, t \quad (8n)$$

$$\sum_{n \in \mathcal{N}/n_1} e_{n\tau} \geq \sum_{t=\tau}^{\tau + T^{\mathrm{crit}}} \sum_{n \in \mathcal{N}/n_1} X^{\mathrm{crit}} \cdot (P_{nt}^{\mathrm{load}} - \overline{P}_{nt}) \Delta T, \forall t \quad (8o)$$

where $\Xi = \{p_{nt}, p_{nt}^{\mathrm{inj}}, q_{nt}, q_{nt}^{\mathrm{inj}}, q_{nt}^+, q_{nt}^-, v_{nt}, p_{nt}^{\mathrm{st}}, e_{nt}, \forall n, t; i_{\ell t}, \forall \ell, t\}$ is the set of optimization variables. The objective function (8a) to be minimized comprises the total active power cost and a penalization of reactive power generation, to reduce the control effort ($C_n^{\mathrm{P}} >> C_n^{\mathrm{Q}}$). Constraint (8b) uses two nonnegative auxiliary variables q_{nt}^+ and q_{nt}^- to decompose the reactive power generation/absorption q_{nt} into two non-negative components and along with the second term of the objective function minimizes the absolute value of reactive power in the distribution grid. Constraints (8c) and (8d) ensure the nodal active and reactive power balance, whereas the set of constraints (8e) and (8f) impose the upper and lower capacity limits at each node for active and reactive power generation, respectively. Constraint (8g) approximates the current flowing in each branch considering only the active power contribution [15], and (8h) imposes the corresponding current flow limits. Similarly, the voltage drop over all branches is approximated by equation (8i) around a known operating voltage point V_n^* [15], whereas constraint (8j) imposes the nodal voltage limits. The used approximations for the current flows (8g) and voltages (8i), are valid for normal grid operation in low voltage (LV) grids, where the R/X ratio of the branches is high (> 2) and the voltage angles are very small ($< 10°$). The interested reader is referred to [15] for more details on these linear approximations.

The set of constraints (8m) - (8n) models the operation and the technical limits of ESS. The state of charge of the ESS at every time period t is modeled by (8k). Constraints (8l) enforce that the state of charge at the beginning and at the end of the optimization horizon are equal to the initial value e_n^0. The upper and lower limits of the state of charge are imposed by (8m), while the charging/discharging process is bounded by the physical capacity limits of the ESS through constraints (8n). The purpose of modelling the charging and discharging ESS operations using the single variable p_{nt}^{st} is twofold: it ensures that no simultaneous charging and discharging is allowed, while it preserves the linear formulation of the problem. As a drawback, conversion losses of the storage are neglected. On the contrary, modeling charging and discharging operations of the ESS using separate variables would require the introduction of either additional binary variables or non-linear constraints in order to guarantee that only one of these operations is allowed during every time period. Furthermore, for the sake of simplicity and to ensure clarity to our paper's scope, we assume a power factor of 1 for the ESS. Constraint

(8o) guarantees the *resiliency* of the distribution system against sudden disconnections from the main grid. In particular, this constraint ensures that the amount of energy stored in energy units is sufficient to cover a critical percentage X^{crit} of the total net load, i.e., active power demand minus local generation, for the following T^{crit} time periods, while operating in an islanded mode. Note that constraint (8o) is applied only to internal nodes of the distribution network, i.e., $n \in \mathcal{N}/n_1$, where n_1 denotes the point of common coupling between the distribution system and the main grid.

It should be noted that the given problem is linear and that an iterative scheme should be used to derive AC feasible solutions, updating the operating point at each iteration. In this paper, we focus on an investment problem, and thus, we choose one fixed voltage operating point V_n^* for the linearization similar to [26]. For more details regarding singe- and three-phase OPF formulations using the BFS approach, we refer the readers to [11] and [28].